Interference evidence for Rashba-type spin splitting on a semimetallic WTe_{2} surface

Qing Li, Jiaqiang Yan, Biao Yang, Yunyi Zang, Junjie Zhang, Ke He, Menghao Wu, Yanfei Zhao, David Mandrus, Jian Wang, Qikun Xue, Lifeng Chi, David J. Singh, and Minghu Pan

Phys. Rev. B **94**, 115419 — Published 13 September 2016

DOI: 10.1103/PhysRevB.94.115419

Interference Evidence for Rashba-Type Spin-Split on Semimetallic WTe_2 Surface

Qing Li[1], Jiaqiang Yan[2,3], Biao Yang[1], Yunyi Zang[4], Junjie Zhang[1], Ke He[4], Menghao Wu[5], Yanfei Zhao[6], David Mandrus[3,4], Jian Wang[6], Qikun Xue[4], Lifeng Chi[1]*, David J. Singh[7,]* and Minghu Pan[5,]*

[1]Institute of Functional Nano & Soft Materials (FUNSOM), Jiangsu Key Laboratory for Carbon-Based Functional Materials & Devices, Soochow University, 199 Ren'ai Road, Suzhou, 215123, Jiangsu, P. R. China.

[2]Department of Materials Science and Engineering, University of Tennessee, Knoxville, Tennessee 37996, USA.

[3]Materials Science and Technology Division, Oak Ridge National Laboratory, Oak Ridge, Tennessee 37831, USA.

[4]State Key Laboratory of Low-Dimensional Quantum Physics, Department of Physics, Tsinghua University, Beijing 100084, China

[5]School of Physics, Huazhong University of Science and Technology, Wuhan 430074, China.

[6]International Center for Quantum Materials, School of Physics, Peking University, Beijing 100871, China

[7]Department of Physics and Astronomy, University of Missouri, Columbia, Missouri 65211-7010, USA

Semimetallic tungsten ditelluride displays an extremely large non-saturating magnetoresistance, which is thought to arise from the perfect n-p charge compensation with low carrier densities in WTe_2. We find a strong Rashba spin-orbit effect in density functional calculations due to the non-centrosymmetric structure. This lifts two-fold spin degeneracy of bands. A prominent Umklapp interference pattern is observed by our scanning tunneling microscopic measurements at 4.2 K, which differs distinctly from the surface atomic structure demonstrated at 77 K. The energy dependence of Umklapp interference shows a strong correspondence with densities of states integrated from ARPES measurement, manifesting a fact that the bands are spin-split on the opposites side of Γ. Spectroscopic survey reveals the electron/hole asymmetry changes alternately with lateral locations along b axis, providing a microscopic picture for double-carrier transport of semimetallic WTe_2. The conclusion is further supported by our ARPES results and Shubnikov-de Haas (SdH) oscillations measurements.

WTe_2, a layered transition-metal dichalcogenide (TMD), whose sheets consist of a tungsten layer sandwiched by adjacent chalcogenide layers, has been the subject of intense interest for its extraordinary magnetoresistance (XMR) [1-6]. The non-saturation of the resistance with magnetic field differs significantly with normal MR phenomenon, where the magnetoresistance

is quadratic only in low fields, and tends to saturate at high fields [1]. This phenomenon has been ascribed to the perfect n-p charge compensation in WTe_2, based on the investigations by angle-resolved photoelectron spectroscopy (ARPES) [7] and theoretical calculations [3]. The two-band model for semimetals implies a sharp resonance with exact compensation (n=p), which results in MR given by $\Delta\rho/\rho=\mu^2B^2$ and ρ_{xx} growing with B^2 without saturation [1,3].

Tungsten chains are formed within dichalcogenide layers along *a* axis of the WTe_2 orthorhombic unit cell, making the compound structurally one dimensional. As a consequence, a quasi-one dimensional, semi-metallic Fermi surface topology of WTe_2 was found along the Γ-X direction [1]. High resolution scanning tunneling microscopy (STM) has been recently used to visualize the surface morphology of WTe_2 and reported a lattice distortion due to surface reconstruction [8]. Very recently, a complicated Fermi surface of WTe_2 was reported via the ARPES measurements [9], in which nine Fermi pockets were resolved. This observation differs from the simple Fermi surface topology (one electron and one hole pocket) significantly. More important, similar to the case of topological insulators [10-12], the circular dichroism that is a signature for strong spin-orbital coupling (SOC) and a spin texture, was observed at the Fermi surface in photoemission spectra [8,9]. Such spin texture provides mechanisms to protect the backscattering at zero fields thus may be responsible for the XMR.

Here we find, in accord with other recent results, a spin splitting of the bands, symmetrical

around the zone center leading to multiple sheets of Fermi surface along the Γ-X direction. The breaking of spin degeneracy is in general possible either from time reversal symmetry breaking, i.e. magnetism, or the combination of spin-orbit and spatial inversion symmetry breaking. WTe_2 is not magnetic, and therefore the splitting must be due to spin-orbit, i.e. the Rashba-Dresselhaus Hamiltonian. We find this splitting in our first principles calculations including spin-orbit, confirming its spin-orbit origin. The splitting as seen is along Γ-X, reflecting the crystal symmetry, which is orthorhombic and not cubic. Therefore, this is Rashba type splitting. The SOC lifts two-fold spin degeneracy of bands across Fermi level (E_F) and produces five Fermi pockets, including two electron pockets, two hole pockets and one deeper hole band that just kisses E_F. In conjunction with scanning tunneling microscopy and spectroscopy (STM/STS) measurements, we observe umklapp-type interference pattern on the surface of *in situ* cleaved WTe_2 single crystal at 4.2 K. Such an umklapp-type interference pattern is a spectroscopic feature instead of pure geometric one. It is dominated by spin-conserving processes, with that a reciprocal lattice vector $\vec{g}$ is permitted, whereas ordinary interferences are forbidden by spin conservation at low temperature. The band splitting is further evidenced by the energy dependence of the interference patterns.

DFT calculations, with the full-potential linearized augmented plane wave (LAPW) WIEN2k package and the PBE exchange-correlation functional [13], were performed to investigate the

WTe_2 bulk structure (see methods for details). Atom positions after relaxation are shown in Supplementary Tab. S1 and the relaxed structure is given in Fig. 1(a). There is an interesting connection between WTe_2 and MoS_2 in that bulk MoS_2 is centrosymmetric, while the single layer version is not, which leads to spin-orbit induced valley effects in MoS_2 [14].

The band structure shown in Fig. 1(b) is in agreement with previous reports [1,15] in showing WTe_2 to be a semimetal with valence and conduction bands that barely cross the Fermi energy at different places in the Brillouin zone along the Γ–X direction. Our calculated band structure is similar on a large scale to that reported previously [1], but differs in details presumably due to the structure used. With SOC, the non-centrosymmetric structure leads to the structure inversion-asymmetric (SIA) spin splitting term in Hamiltonian, *i.e.* a Rashba effect [16-18]. Importantly, the splittings are large enough to give visibly different Fermi surfaces (Fig. 1(d)). There are five non-degenerate bands crossing the Fermi level: two electron bands, two hole bands and one deeper hole band that just kisses E_F to give very tiny hole sections. A closer inspection of the calculated low-lying electronic structure in the Γ–X direction is illustrated in Fig. 1(c) (right panel), showing that an original set of electron and hole bands with spin degeneracy splits into two sets of electron and hole bands. The two large hole sheets of the Fermi surface are connected across the zone center, while the two electron sheets have small necks along the k_z direction (Fig. 1(d)). Importantly, the low energy structure is not reasonably characterized as one or even two

dimensional. The calculated plasma energies in the three crystallographic directions are $\Omega_{p,x}$=1.07 eV, $\Omega_{p,y}$=0.83 eV and $\Omega_{p,z}$=0.62 eV, which would predict a constant scattering time conductivity anisotropy of $\sigma_x/\sigma_z \sim (\Omega_{p,x}/\Omega_{p,z})^2$ of approximately 3 and similarly σ_x/σ_z of approximately 1.7, *i.e.* a moderately anisotropic three dimensional semimetal.

The five pockets of the Fermi surface (Fig. 1(d)) lie along the Γ-X direction, which is supported by SdH oscillations (see Fig. S1 for details) measured with perpendicular field (H//c axis) [19]. ARPES measurements (left panel of Fig. 1(c)) resolve three bands across E_F along Γ-X, referred as α, β and δ bands, respectively (see methods and Fig. S2 for details). The β and δ bands contribute two Fermi crossings along Γ-X and forms the two hole pockets. The α band gives two Fermi crossings and forms an electron pocket. Two bands are found to be located around 80 meV (the γ band) and 190 meV (the ε band) below E_F. Therefore, except for the tiny hole pocket inside of hole dumbbells, all four Fermi pockets predicted by our DFT calculations are clearly resolved.

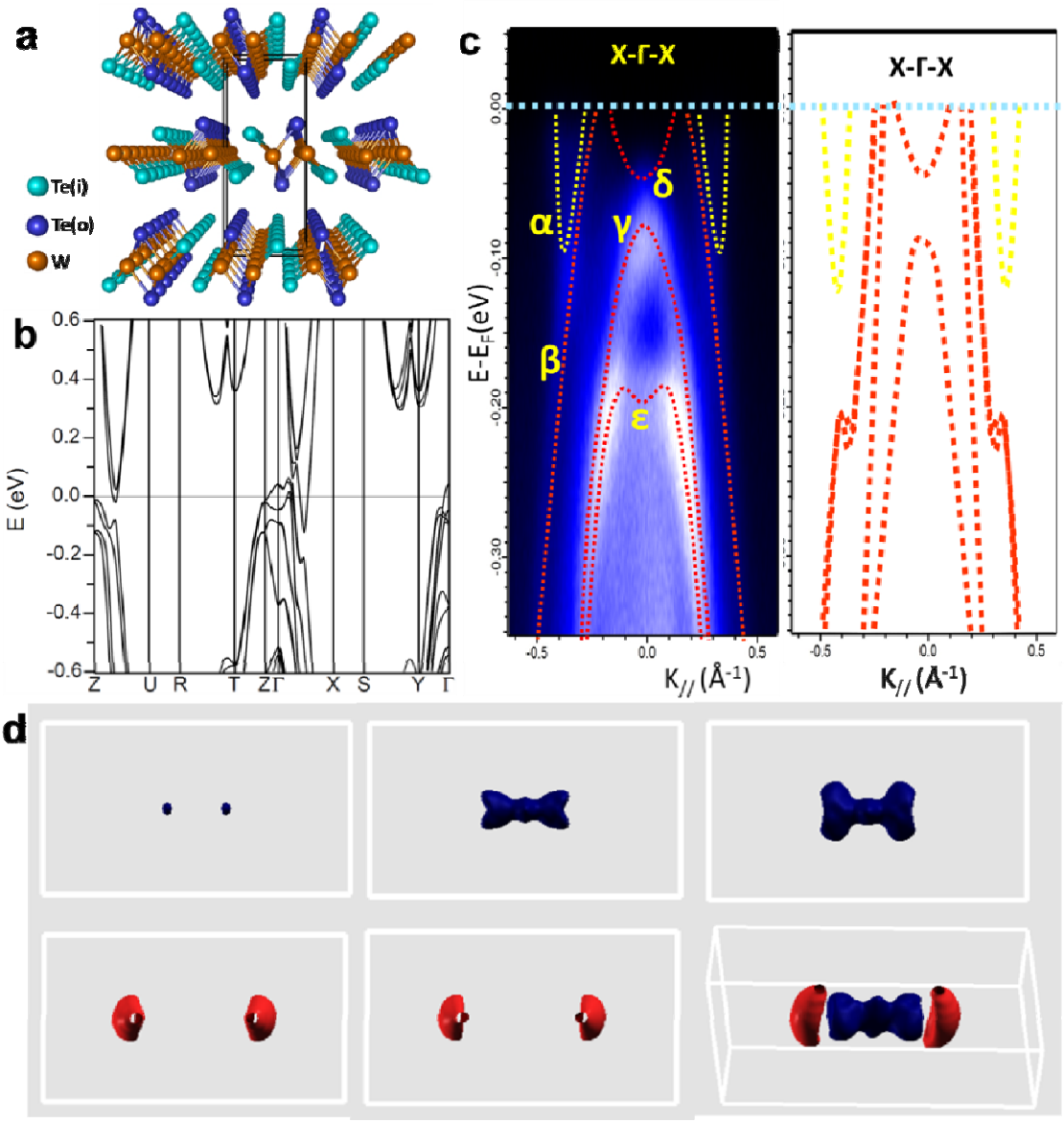

FIG. 1. Calculated electronic structures of WTe_2. (a) The relaxed bulk structure of WTe_2. (b) The calculated band structure of WTe_2 bulk, with relaxed structure of the slab. (c) The photoemission intensity plot (left panel) along Γ-X direction together with a closer inspection of the calculated electronic structure (right panel). The colorful lines are the schematic drawings of the low-lying electronic structure of WTe_2. (d) Calculated 3D Fermi surface for WTe_2

bulk. Fermi surfaces for the five bands crossing the Fermi level shown as blue for hole surfaces and red for electron surfaces. The bottom right panel shows the total Fermi surface.

In the topological insulators, SOC induces the spin texture in the topologically protected surface states, namely opposite spin direction on the opposite side of Γ, which provides the protection against backscattering in the absence of magnetic scattering at zero field [20-22]. Although the existence of spin texture in WTe_2 has been detected by ARPES measurements [9], a direct observation of spin-texture and its dependence with external magnetic field are still missing. For this purpose, extensive STM/S measurements were performed.

Figure 2(a) shows a representative topographic image of a fresh-cleaved WTe_2 surface obtained at 77 K. Based on crystal-chemical considerations and experience with other layered TMDs such as $MoSe_2$ and $IrTe_2$ [23,24], cleavage occurs between adjacent chalcogenide layers so that Te terminated surfaces are exposed. On the surface of WTe_2, the tellurium octahedra distort slightly and the metal atoms are displaced from their ideal octahedral sites, forming zigzag metal-metal chains along *a* axis (Fig. 2(b)). The Te atom layers are buckled with the Te(i) atoms displaced a little into the sandwich layer and Te(o) atoms moved slightly out. We therefore assign the brighter feature in Fig. 2(a) to Te(o) atoms while the darker ones to Te(i) atoms.

Figure 2(c) gives the calculated total DOS for WTe_2 bulk and the projections of the electronic density of states (PDOS) onto W (d bands) and Te (p bands) atoms. Both W (d orbitals) and Te (p

orbitals) contribute to the overall DOS of valence and conduction bands. In order to investigate the electronic structure of the WTe_2 surface, conductance spectra (*dI/dV* versus V_b), which measure the local density of states (DOS) at the tip site, were obtained. Thousands of tunneling spectra were acquired on clean WTe_2 surface at different locations (cyan curves in Fig. 2(d)) and an averaged *dI/dV* spectrum is superposed (shown as black curve in Fig. 2(d)), which are in excellent agreement with the theoretical calculations. Without the consideration of the spin, the electronic structure of WTe_2 around E_F is fairly simple: The valence band and conduction bands barely cross the Fermi energy at different places in the Brillouin zone (a schematic scratch of the band structure of WTe_2 is shown in the insert of Fig. 2(d)). We then are able to identify an E_{CBM} (conduction-band minimum) at ~-40 mV and an E_{VBM} (valence-band maximum) at +40~+60 mV. The overlap between the valence band and conduction bands is 80 meV to 100 meV, leading to the semimetallic nature of the sample. The spectroscopic results agree reasonably well with our band structure calculations and ARPES measurements [7].

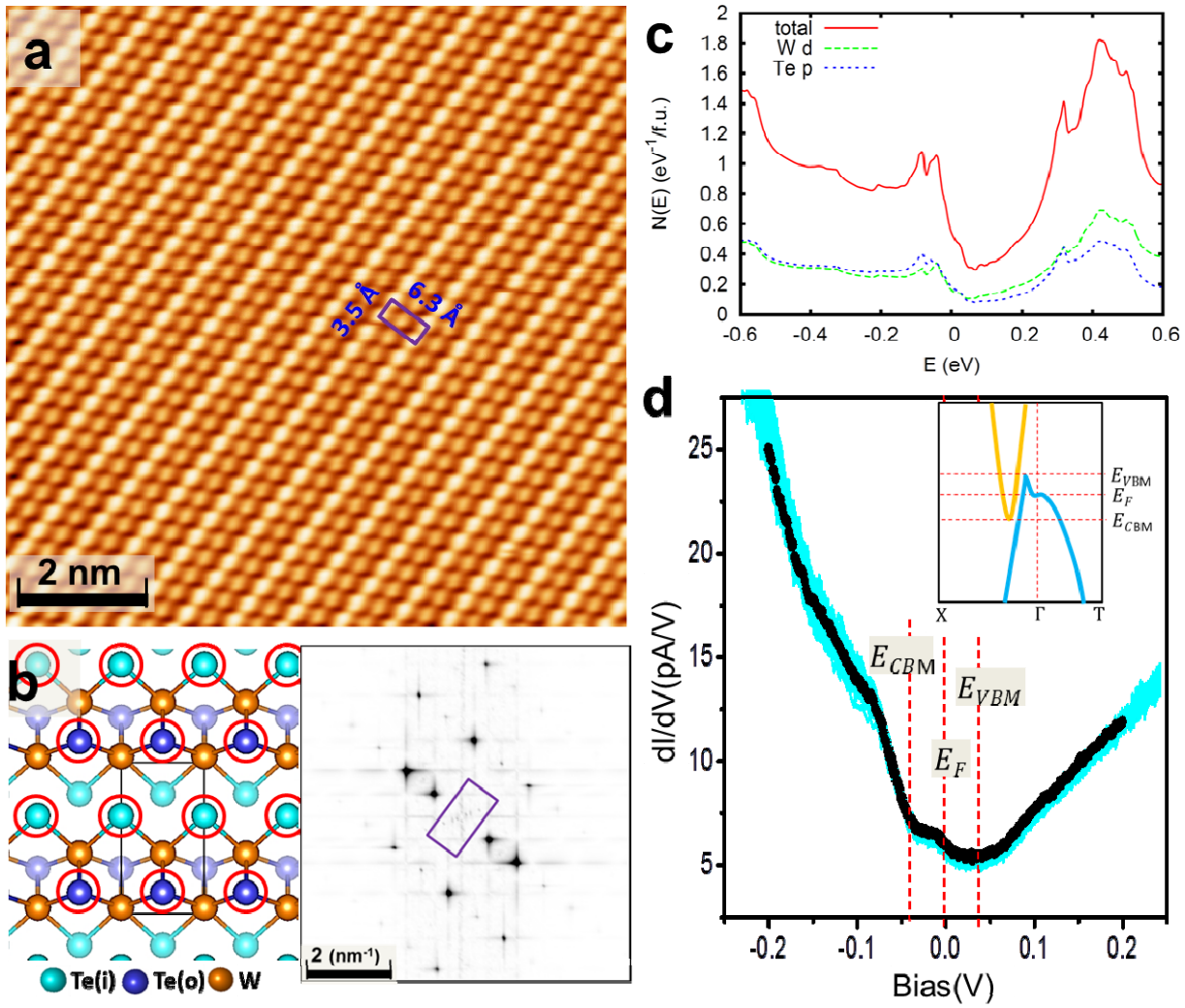

FIG. 2. STM/S measurements of cleaved WTe_2. (a) Atomically resolved STM topographic image of the cleaved WTe_2 surface acquired at 77 K. (b) Top view of crystal structure of WTe_2. Top Te(i) and Te(o) atoms are highlighted by red circles. (Right panel) FFT image of (a), displaying Bragg vectors and the corresponding first Brillouin zone (purple rectangle). (c) The calculated total DOS, with projections of the DOS onto different atoms, W (d obitals) and Te (p obitals). The energy zero is set to the Fermi level. (d) *dI/dV* spectrum acquired on the WTe_2 surface. Setpoint parameters: V_b = +50 mV (a), R_J = 0.5 GΩ; V_{rms} = 5 mV. (Inset) schematic band structure of WTe_2.

Dramatic changes take place when the sample is cooled down to 4.2 K, at which STM images of the surface exhibit a unique "lattice" pattern (Fig. 3(a)). The size of unit cell for this phase is 3.5×6.3 Å, exactly the same as the unit cell of the WTe_2 surface taken at 77 K. Quite obviously, the darker protrusions shift from the center (77 K) to the edge (4.2 K) of the unit cell and form a rectangular lattice instead of the triangular one at 77 K (left panel of Fig. 3(b)). Note that no structural transition has been reported for WTe_2 in this temperature range and actually a structural change for the top Te layer is extremely energetically unfavorable. We calculate the energies of three different structures for top Te-W-Te trilayer, including 1T, 1T' (the most stable configuration for WTe_2) and an artificial model named as 1T". Only the structure of 1T" could give a rectangular tungsten lattice, but its energetic cost is extremely high as 0.28 eV per atom. Therefore, the rectangular lattice at 4.2 K should represent electronic variations on the surface.

The observed "lattice" pattern cannot be assigned to the charge ordering since no gap opening is obtained (Fig. 2(d)) [25-28]. Alternatively, the phase transition can be a result of the quasi-particle interference (QI) induced by surface Rashba SOC splitting. It is vital to realize that states with $\overrightarrow{k_F}$ and $-\overrightarrow{k_F}$ have opposite spin directions. All of the interference processes building up the FS topology should be forbidden in the absence of spin-flip [29]. One the other hand, in the umklapp-type interference processes, a reciprocal lattice vector $\vec{g}$ are not forbidden by spin. For example, interference between ($\vec{k}$, ←) and ($\vec{k}+\vec{g}$, ←) is permitted, while interference between

($\vec{k}$,←) and (-$\vec{k}$,→) is NOT allowed (Fig. 3(b), right panel). As a consequence, the presence of defect is not necessary for the scattering and the pattern is formed extending the entire sample surface where a regular crystalline lattice of WTe_2 preserved, as that reported for the Be(110) surface [30].

The umklapp-type interference processes are further evidenced by differential conductance mapping at different energy levels. The differential conductance maps taken with sample bias varying from -0.4 V to 0.5 V are shown in Supplementary Fig. S3 and a representative *dI/dV* mapping at -0.1 V is given in Fig. 3(c), together with the corresponding fast Fourier transform (FFT) image (Fig. 3(d)). As we know, dI/dV map is a spatial visualization for the distribution of electronic density of states by removing the topographic effect. The $\overrightarrow{g_a}$ and $\overrightarrow{g_b}$ in Fig. 3(d) do not always exist, especially for some bias energies. For example, when the bias is below -400 meV, only an unidirectional stripe pattern is visible at the *dI/dV* map, manifesting an interference with a reciprocal lattice vector $\overrightarrow{g_b}$, where $\overrightarrow{g_a}$ and $\overrightarrow{g_a} + \overrightarrow{g_b}$ are missing in its FFT image. Even the vector $\overrightarrow{g_b}$ also becomes very weak at -0.4 eV. With the increment of the bias, QI patterns show the interference with reciprocal lattice vectors not only along the Γ-X direction, but also for the Γ-Y direction. The intensity of interference pattern with the reciprocal lattice vector $\overrightarrow{g_b}$ reaches the maximum at -200 meV, while with $\overrightarrow{g_a}$ has a maximum at around -100 meV, as illustrated in Fig. 3(e). The result of strong energy-dependence of dI/dV patterns presented here suggests an

electronic origin of $\overrightarrow{g_a}$ and $\overrightarrow{g_b}$ vectors, instead of atomic-resolved structural feature. The appearance of $\overrightarrow{g_a}$ and $\overrightarrow{g_b}$ vectors can be explained as the result of umklapp-type interference on the surface dominated by spin-conserving processes.

By comparing with the integrated DOS from our ARPES measurement (Fig. 3(f)), a coincidence was found, showing that the interference maxima for reciprocal lattice vectors always occur at the top/bottom of downwards γ, ε bands or upwards band α. Such coincidence manifests those downwards/upwards bands are spin-split, namely opposite spin direction on the opposite side of Γ in momentum space. If the bands are non-spin-splitting, the Fourier transform of STM dI/dV maps near E_F, will show the image of two-dimensional Fermi contours with high intensities at $2k_F$ [31-33]. It will not give lattice-like spots with that the reciprocal lattice vectors $\vec{g}$ are permitted, as we observed in our experiments. Once the bands become spin-splitting, states with k_F and $-k_F$ have opposite spin directions. Ordinary interferences building up the Fermi surface topology in the FFT maps should be forbidden at very low temperature by spin-conservation processes [34]. Only the spin-conserving interferences are permitted and the energy dependence of such spin-conserving patterns has to be coincident with the maxima of the spin-splitting bands. Our observation gives a spatially visualized picture of the "spin texture", which agrees with Jiang *et al.*'s circular dichroism (CD) measurement [9].

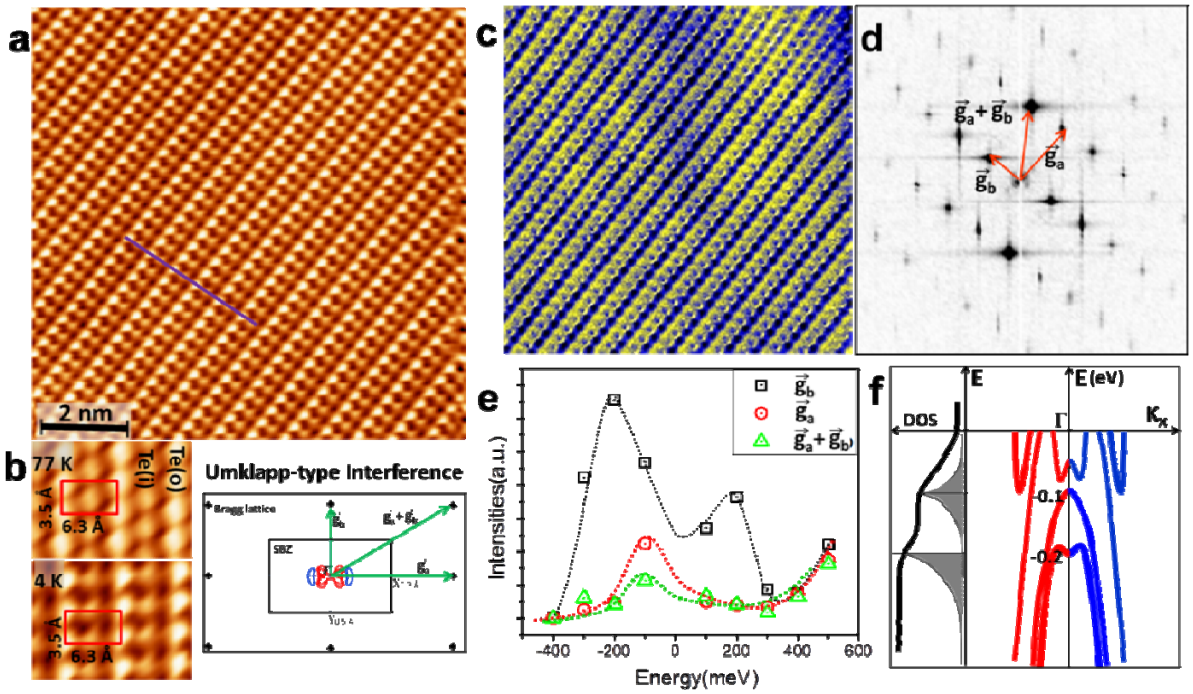

FIG. 3. STM images and tunneling spectra obtained at 4.2 K. (a) STM topographic image, V_b =500 mV, I=100 pA. (b) (Left) STM images taken at 77 K and 4.2 K. (Right) Schematic drawing showing umklapp-type interference processes in spin-conserving processes. (c) dI/dV image with V_b =-100 mV, I=100 pA. The size of image is 10 nm×10 nm. (d) FFT pattern of the image shown in panel (c). (e) The energy dependence of the intensities for vector , and + , respectively. (f) A schematic illustration for bands near E_F along Γ-X direction with the integrated DOS (thick black line) from ARPES data.

Due to the surface enhanced Rashba SOC, the origin of the degenerate band is shifted by k_R, but in opposite directions for up- and down-spins with in overall spin-orbit lowering of Δ_R energy. This Rashba type spin orbit splitting is k-dependent, but is about 50 meV at some k, and lower at others. When the measuring temperature T_m is raised *i.e.* at 77 K, the peculiar

interference pattern vanishes and an STM image representing the surface geometry is observed, meaning that scattering processes have sufficient energy mix bands at different energy, removing the spin protection from scattering; conversely at low T, the STM image will be dominated by such interference pattern, as what we observed at 4.2 K.

A spectroscopic survey was taken to study the DOS distributions on surface. Figure 4(a) shows 50 differential tunneling conductance spectra acquired within five UCs (marked by a blue line in Fig. 3(a)). All curves exhibit similar line shapes without evidence for an energy gap. From the spatial mapping this series of spectra (Fig. 4(b)), DOS oscillation of both filled states and empty states with lateral displacement, is clearly observed. The maximum position of filled states does not meet with the maximum of empty states and the separation between the lateral positions of the maxima for empty and filled states is about 2 Å, manifesting a separation of electron/hole-like channels.

It has been proposed that particle-hole asymmetry arises from an imbalance between the tunneling rate for electron injection and extraction [35,36], and this mechanism has been widely applied in the high-Tc cuprate superconductors studies [37,38]. The ratio of particle-hole asymmetry R($\vec{r}$) can be given by $R(\vec{r}) = \frac{\int_0^{E_2} N(\vec{r},E)dE}{\int_{-E_1}^{0} N(\vec{r},E)dE}$ [36]. By integrating empty and filled states from -0.2 V to 0 and from 0 to 0.4 V, respectively, a normalized particle/hole asymmetry ratio is calculated, as shown in Fig. 4(c). The electron/hole ratio is varying within a unit cell along *b* axis,

which is perpendicular to tungsten chain. The overall electron/hole ratio within a unit cell equals to one, with *R* lower than one (electron-like) in half of the unit cell and vice versa in another half, suggesting the perfect n-p charge compensation in WTe_2 [1,3]. As far as we know, such a microscopic picture of separated electron/hole channels for a double-carrier system has not been observed previously for semimetallic materials.

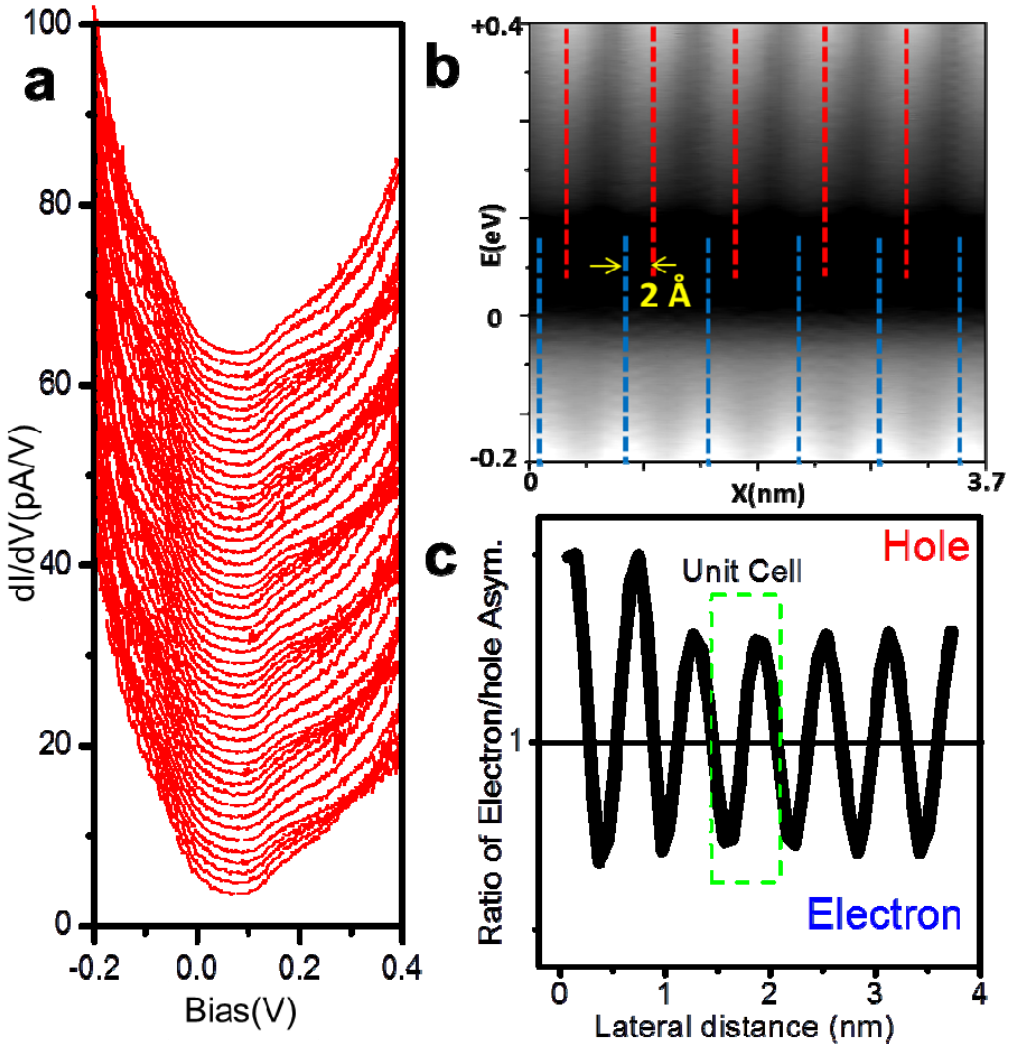

FIG. 4. *dI/dV* spectra obtained at 4.2 K. (a) A series of *dI/dV* spectra acquired along the blue line in Fig. 3(a). V_b =50 mV, *I*=100 pA, V_{rms} = 5 mV. (b) A gray-scale plot of these *dI/dV* curves with the tip displacement. (c) The calculated ratio of electron/hole asymmetry based on the spectra survey in panel (a).

Finally, we checked the electronic properties of WTe_2 surface under applied perpendicular magnetic field. As shown in Fig. S4(a), no distinct change in the spectrum is observed upon applying magnetic fields from 0 to 8 T. Detail analysis of the spectroscopy behavior under magnetic field can be found in Fig. S4.

In summary, STM/S, ARPES and transport measurements, corroborated by DFT calculations, reveal that strong Rashba type spin-orbit effects due to the non-centrosymmetric structure substantially split the electron and hole bands crossing the Fermi level and lift the spin degeneracy of these bands. The band structure is not reasonably described as one dimensional and is instead three dimensional in nature. Low temperature STM/S measurements show an umklapp-type interference pattern on WTe_2 surface at 4.2 K, proven to be a spectroscopic feature instead of a pure geometric one, which is dominated by spin-conserving processes. Spectroscopic surveys reveal that the ratio of electron/hole asymmetry changes alternately with lateral locations along *b* axis, while the overall electron/hole ratio within a unit cell stays in balance. In WTe_2 the Fermi surface is arranged along the a-axis which is the current direction for the XMR and the direction in which the Rashba-type splitting are important. The inversion symmetry is broken by

a lack of reflection in the c-direction. This leads to an important spin texture in the *a-b* plane, as was discussed by Jiang and co-workers based on ARPES [9]. Thus the magnetic field along *c* breaks this texture. We infer that it is this that enables scattering between parts of the Fermi surface that have different spin without field and underlies the XMR effect. Our findings provide a microscopic atomic level understanding of the electronic and spin structure of the exotic semimetal material WTe_2 and show the importance of the interplay of spin-orbit interactions with the non-centrosymmetric crystal structure.

We acknowledge Collaborative Innovation Center of Suzhou Nano Science & Technology, the Priority Academic Program Development of Jiangsu Higher Education Institutions. QL and LFC acknowledge the financial supported by the Major State Basic Research Development Program of China (2014CB932600), National Natural Science Foundation of China (91545127, 91227201 and 21403149). DGM acknowledges support from the Gordon and Betty Moore Foundation (GBMF4416). Work at the University of Missouri (DFT calculations) was supported by the U.S. Department of Energy, Basic Energy Sciences, Materials Sciences and Engineering Division, through the MAGICS center Work at ORNL was supported by the Department of Energy, Basic Energy Sciences, Materials Sciences and Engineering Division.

*mhupan@gmail.com; chilf@suda.edu.cn; singhdj@missouri.edu

[1] M. N. Ali, J. Xiong, S. Flynn, J. Tao, Q. D. Gibson, L. M. Schoop, T. Liang, N. Haldolaarachchige, M. Hirschberger, N. P. Ong, and R. J. Cava, Nature **514**, 205 (2014).

[2] L. P. He, X. C. Hong, J. K. Dong, J. Pan, Z. Zhang, J. Zhang, and S. Y. Li, Phys. Rev. Lett. **113**, 246402 (2014).

[3] H. Y. Lv, W. J. Lu, D. F. Shao, Y. Liu, S. G. Tan, and Y. P. Sun, Euro. phys. Lett. **110**, 37004 (2015).

[4] P. L. Cai, J. Hu, L. P. He, J. Pan, X. C. Hong, Z. Zhang, J. Zhang, J. Wei, Z. Q. Mao, and S. Y. Li, Phys. Rev. Lett. **115**, 057202 (2015).

[5] X. C. Pan, X. L. Chen, H. M. Liu, Y. Q. Feng, Z. X. Wei, Y. H. Zhou, Z. H. Chi, L. Pi, F. Yen, F. Q. Song, X. G. Wan, Z. R. Yang, B. G. Wang, G. H. Wang, and Y. H. Zhang, Nat. Commun. **6**, 7805 (2015).

[6] D. F. Kang, Y. Z. Zhou, W. Yi, C. L. Yang, J. Guo, Y. G. Shi, S. Zhang, Z. Wang, C. Zhang, S. Jiang, A. G. Li, K. Yang, Q. Wu, G. M. Zhang, L. L. Sun, and Z. X. Zhao, Nat. Commun. **6**, 7804 (2015).

[7] I. Pletikosić, M. N. Ali, A. V. Fedorov, R. J. Cava, and T. Valla, Phys. Rev. Lett. **113**, 216601 (2014).

[8] P. Kumar Das, D. Di Sante, I. Vobornik, J. Fujii, T. Okuda, E. Bruyer, A. Gyenis, B. E. Feldman, J. Tao, R. Ciancio, G. Rossi, M. N. Ali, S. Picozzi, A. Yadzani, G. Panaccione and R. J. Cava, Nat. Commun. DOI: 10.1038/ncomms10847 (2016).

[9] J. Jiang, F. Tang, X. C. Pan, H. M. Liu, X. H. Niu, Y. X. Wang, D. F. Xu, H. F. Yang, B. P. Xie, F. Q. Song, P. Dudin, T. K. Kim, M. Hoesch, P. K. Das, I. Vobornik, X. G. Wan, and D. L. Feng, Phys. Rev.

Lett. **115**, 166601 (2015).

[10] J. Jiang, S. Li, T. Zhang, Z. Sun, F. Chen, Z. R. Ye, M. Xu, Q. Q. Ge, S. Y. Tan, X. H. Niu, M. Xia, B. P. Xie, Y. F. Li, X. H. Chen, H. H. Wen, and D. L. Feng, Nat. Commun. **4**, 3010 (2013).

[11] S. R. Park, J. Han, C. Kim, Y. Y. Koh, C. Kim, H. Lee, H. J. Choi, J. H. Han, K. D. Lee, N. J. Hur, M. Arita, K. Shimada, H. Namatame, and M. Taniguchi, Phys. Rev. Lett. **108**, 046805 (2012).

[12] D. Hsieh, Y. Xia, D. Qian, L. Wray, J. H. Dil, F. Meier, J. Osterwalder, L. Patthey, J. G. Checkelsky, N. P. Ong, A. V. Fedorov, H. Lin, A. Bansil, D. Grauer, Y. S. Hor, R. J. Cava, and M. Z. Hasan, Nature **460**, 1101 (2009).

[13] P. Blaha, K. Schwarz, G. Madsen, D. Kvasnicka, and J. Luitz, (Technische Univ. Wien, 2001).

[14] X. D. Xu, W. Yao, D. Xiao, and T. Heinz, Nat. Phys. **10,** 343 (2014).

[15] J. Augustin, V. Eyert, T. Boker, W. Frentrup, H. Dwelk, C. Janowitz, and R. Manzke, Phys. Rev. B **62**, 10812 (2000).

[16] E. I. Rashba, Sov. Phys. Solid State. **2**, 1109 (1960).

[17] Y. A. Bychkov, and E. I. Rashba, J. Phys. C **17**, 6039 (1984).

[18] Y. A. Bychkov, and E. I. Rashba, JETP Lett. **39**, 78 (1984).

[19] Y. F. Zhao, H. W. Liu, J. Q. Yan, W. An, J. Liu, X. Zhang, H. C. Wang, Y. Liu, H. Jiang, Q. Li, Y. Wang, X. Z. Li, D. Mandrus, X. C. Xie, M. H. Pan, and J. Wang, Phys. Rev. B **92**, 041104(R) (2015).

[20] P. Roushan, J. Seo, C. V. Parker, Y. S. Hor, D. Hsieh, D. Qian, A. Richardella, M. Z. Hasan, R. J.

Cava, and A. Yazdani, Nature **460**, 1106 (2009).

[21] T. Zhang, P. Cheng, X. Chen, J. F. Jia, X. C. Ma, K. He, L. L. Wang, H. J. Zhang, X. Dai, Z. Fang, X. C. Xie, and Q. K. Xue, Phys. Rev. Lett. **103**, 266803 (2009).

[22] Z. Alpichshev, J. G. Analytis, J. H. Chu, I. R. Fisher, Y. L. Chen, Z. X. Shen, A. Fang, and A. Kapitulnik, Phys. Rev. Lett. **104**, 016401 (2010).

[23] Q. Li, W. Z. Lin, J. Q. Yan, X. Chen, A. G. Gianfrancesco, D. J. Singh, D. Mandrus, S. V. Kalinin, and M. H. Pan, Nat. Commun. **5**, 5358 (2014).

[24] B. Chamlagain, Q. Li, N. J. Ghimire, H. J. Chuang, M. M. Perera, H. G. Tu, Y. Xu., M. H. Pan, D. Xiao, D. Mandrus, and Z. X. Zhou, ACS Nano **8**, 5079 (2014).

[25] A. Soumyanarayanan, M. M. Yee, Y. He, J. van Wezel, D. J. Rahn, K. Rossnagel, E. W. Hudson, M. R. Norman, and J. E. Hoffman, Proc. Natl. Acad. Sci. USA **110**, 1623 (2013).

[26] M. R. Norman, D. Pines, and C. Kallin, Adv. Phys. **54**, 715 (2005).

[27] S. A. Kivelson, I. P. Bindloss, E. Fradkin, V. Oganesyan, J. M. Tranquada, A. Kapitulnik, and C. Howald, Rev. Mod. Phys. **75**, 1201 (2003).

[28] G. Grüner, Density waves in solids. (Addison-Wesley, 1994).

[29] L. Petersen, and P. Hedegård, Surf. Sci. **459**, 49 (2000).

[30] J. I. Pascual, G. Bihlmayer, Y. M. Koroteev, H. P. Rust, G. Ceballos, M. Hansmann, K. Horn, E. V. Chulkov, S. Blugel, P. M. Echenique, and P. Hofmann, Phys. Rev. Lett. **93**, 196802 (2004).

[31] P.T. Sprunger, L. Petersen, E.W. Plummer, E. Lægsgaard, and F. Besenbacher, Science **275**, 1764 (1997).

[32] Ph. Hofmann, B.G. Briner, M. Doering, H.-P. Rust, E.W.Plummer, and A.M. Bradshaw, Phys. Rev. Lett. **79**, 265(1997).

[33] L. Petersen, P.T. Sprunger, Ph. Hofmann, E. Lægsgaard, B.G. Briner, M. Doering, H.-P. Rust, A.M. Bradshaw, F. Besenbacher, and E.W. Plummer, Phys. Rev. B **57**, R6858(1998).

[34] Y. M. Koroteev, G. Bihlmayer, J. E. Gayone, E.V. Chulkov, S. Blugel, P.M. Echenique, and Ph. Hofmann, Phys. Rev. Lett. **93**, 046403 (2004).

[35] P. W. Anderson, and N. P. Ong, J. Phys. Chem. Solids. **67**, 1 (2006).

[36] M. Randeria, R. Sensarma, N. Trivedi, and F. Zhang, Phys. Rev. Lett. **95**, 137001 (2005).

[37] Y. Kohsaka, C. Taylor, K. Fujita, A. Schmidt, C. Lupien, T. Hanaguri, M. Azuma, M. Takano, H. Eisaki, H. Takagi, S. Uchida, and J. C. Davis, Science **315**, 1380 (2007).

[38] Y. Kohsaka, C. Taylor, P. Wahl, A. Schmidt, J. Lee, K. Fujita, J. W. Alldredge, K. McElroy, J. Lee, H. Eisaki, S. Uchida, D. H. Lee, J. C. Davis, Nature **454**, 1072 (2008).